

AIAA 2001–2209

UNSTEADY BLADE RESPONSE: THE BVI MODEL VS. THE GUST MODEL

Sheryl M. Grace Department of Aerospace and Mechanical Engineering Boston University, 110 Cummington St., Boston, MA 02215. sgrace@bu.edu

7th AIAA/CEAS Aeroacoustics Conference

May 28-30, 2001/Maastricht, The Netherlands

UNSTEADY BLADE RESPONSE: THE BVI MODEL VS. THE GUST MODEL

Sheryl M. Grace*

Department of Aerospace and Mechanical Engineering Boston University, 110 Cummington St., Boston, MA 02215. sgrace@bu.edu

The prediction of unsteady blade response to a flow disturbance using a two-dimensional boundary element method is described. Boundary element analysis of the blade vortex interaction (BVI) problem with both free vortex evolution and fixed vortex convection leads to insights concerning the use of rapid distortion theory (RDT) based methods, such as the gust model, for fluid-structure interaction prediction. In particular, cut-off parameters are determined past which a model based on RDT cannot be used to predict BVI correctly. It is also shown that the reduction in lift response with increasing blade thickness that has been noted experimentally, but not predicted by gust based models, is captured using a free vortex evolution BVI simulation. Therefore this reduction can be attributed to an increased asymmetry in the induced downwash on the pressure and suction sides of the blade section that occurs as the section thickness increases.

Introduction

"NSTEADY blade response has been a focus of research for many years because of its association with blade fatigue and sound generation. Some systems affected by this phenomenon include turbomachinery compressors and turbines, propellers, and helicopter rotors. A simplified model of the fluid-structure interaction problem inherent in these systems consist of a two-dimensional blade section (span neglected) in a fixed (non-rotating) frame of reference surrounded by an inviscid fluid. For underwater applications one can additionally assume the fluid is incompressible. The fluid disturbance is often modeled as either a gust or a passing vortex. The gust representation treats separately each individual Fourier components of the flow disturbance. Moreover, the three directions of the flow disturbance are uncoupled. The unsteady disturbance can also be modeled as a potential vortex, a cloud of vortices, or the computed wake of an upstream body. These models are all referred to as blade-vortex interaction (BVI) models in this paper.

BVI and Gust Problems

A general picture of the BVI problem is given in Figure 1. A single vortex follows a path from upstream, past the blade section, and proceeds downstream. A wake is shed continuously and the strength of the dipole along the wake (not apparent in the figure) is proportional to the change in lift at every time step. The figure depicts the total path followed by the vortex and the wake path. The insert in the top figure shows the lift response as a function of time and is aligned such that the response as the vortex passes the blade section is easily assessed. The lower figure shows the spectral magnitudes ob-



Copyright © 2001 by Sheryl M. Grace. Published by the American Institute of Aeronautics and Astronautics, Inc. with permission.

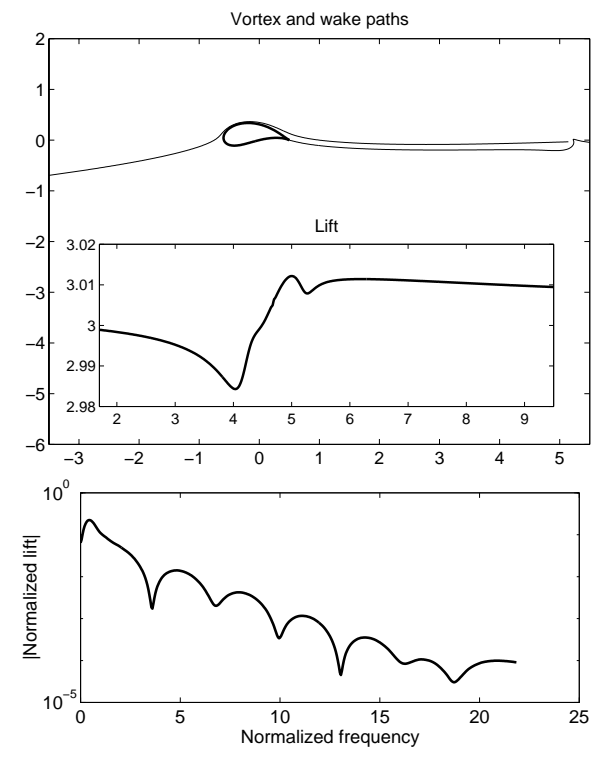


Fig. 1 BVI Problem. Time domain response (top). Frequency domain response (bottom).

tained from a Fourier transform of the time domain response.

The helicopter literature includes hundreds of papers which describe computations based on BVI models. A few relevant ones are cited here. ¹⁻³ The BVI based computations are most often performed in the time domain. ⁴

A sketch of the gust model is shown in Figure 2. Here a flow disturbance is decomposed into its spatial Fourier modes where the amplitude of the disturbance vector is \vec{a} and the wave number vector is \vec{k} . The lift response of a flat-plate airfoil expe-

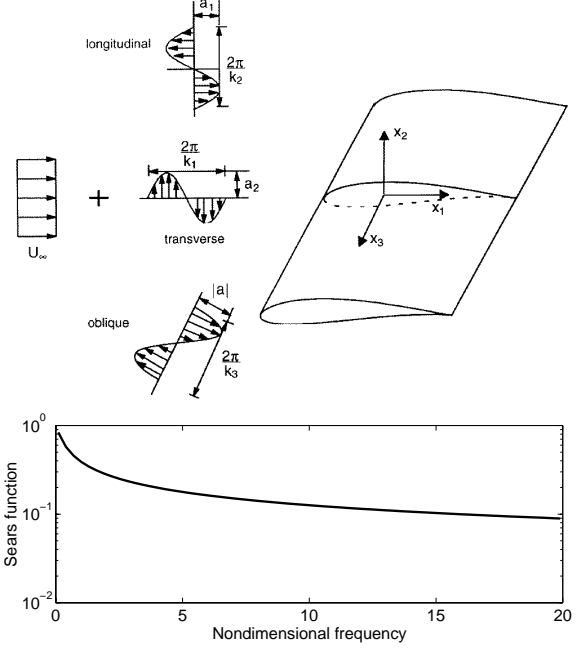


Fig. 2 Gust problem.

riencing a transverse gust (i.e. $a_1 = a_3 = 0$) is proportional to the Sears function

$$S(k) = \frac{2}{\pi k (H_0^2(k) - iH_1^2(k))}.$$
 (1.1)

where H_{ν} is the Hankel function of order ν . This function is shown in Figure 2. Single blade section computations that rely on this disturbance description are frequently carried out in the frequency domain^{5,6} however, [Ref.7,8] are examples of time domain calculations.

For a flat plate airfoil, the BVI and gust problems are virtually the same. The gust disturbance has the form

$$a_2 e^{ik_1(x_1-Ut)}$$

in the frequency domain and the BVI disturbance has the form

$$v_2 e^{-k_1 h} e^{ik_1(x_1 - Ut)}$$

where h in the BVI disturbance is the distance from the vortex to the camberline of the chord at its closest approach to the blade. For example, in Figure 3 the dot on the vortex trajectories path indicates the point at which it is closest to the blade surface. For a flat plate airfoil, this distance would be exactly the distance to the mean camber line of the airfoil. For the thick symmetric airfoil shown in the figure, the distance h is different than the closest approach difference by an amount that is close to the thickness of the airfoil at that point. The bottom figure shows the response spectrum as the solid line. When the spectrum is scaled with the factor $e^{k_1h} = e^{k_10.1}$ one

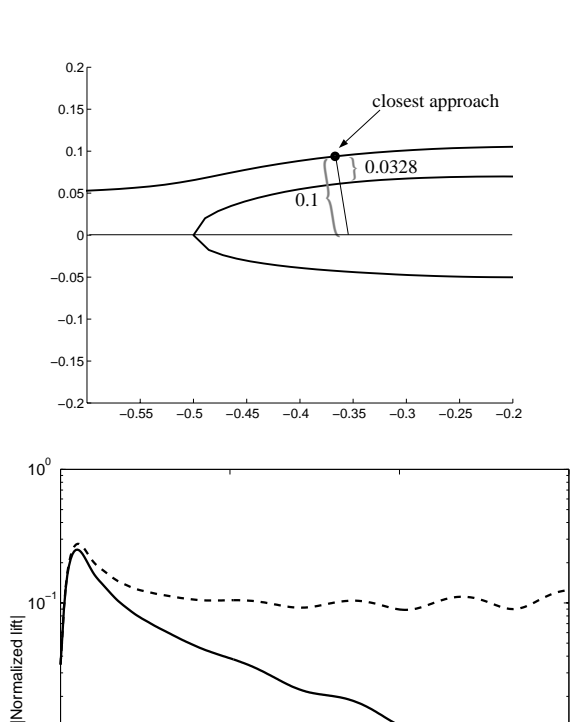


Fig. 3 Top: Closest approach and distance h schematic. (NACA 0012). Bottom: Lift spectrum (solid) lift scaled by the exponential factor (dashed).

Normalized frequency

obtains the dashed line in the figure. It is clear from this example that the high frequency decay is based on the distance from the vortex closest approach location to the mean camber line.

Articles reporting gust based predictions of blade response to flow disturbances have often shown that thickness effects are negligible.^{5,6,8} However, experiments^{9,10} and articles describing BVI computations have shown otherwise. Two reasons for this discrepancy will be discussed in this paper. First, if the flow disturbance magnitude is large, the BVI computations can include nonlinear motion of the passing vortex as opposed to a gust based model which relies on rapid distortion theory (RDT). Second, the inherent asymmetry in the unsteady surface pressure from pressure to suction side² that occurs as thickness increases is not predicted with the usual application of the gust based model but is inherent in the BVI model. In particular, this asymmetry can ony be captured with a gust based model that includes the effect of multiple longitudinal disturbances in conjunction with each transverse disturbance.

10

Computational Method

The present research uses a two-dimensional adaptation of the boundary element method (BEM) as formulated for quasi-potential flows by Morino et. al. 11,12 to solve the two-dimensional BVI problem. The flow is modeled as potential everywhere outside of the solid blade section and outside the wake. Fully attached, high Reynold's number flows are assumed such that viscous effects are prevalent only in the wake generation at the trailing edges of the blade section. The flow velocity infinitely far from the blade section is taken to be uniform in the x_1 direction and to be incompressible.

Under the above assumptions, with the added generalization of compressible flow, the perturbation velocity potential is known to satisfy the convective wave equation¹³

$$M^{2} \frac{D_{\infty}^{2} \phi}{Dt^{2}} - \nabla^{2} \phi = 0, \qquad (2.1)$$

where space and time have been scaled by the reference chord length c and the convective time scale c/U_{∞} , respectively. The solution to Eq. (2.1) satisfies the boundary integral equation

$$-\frac{1}{2\pi} \int\limits_{\tilde{S}} \left[\ln r \frac{\partial \tilde{\phi}(\tilde{\mathbf{y}}, \tau)}{\partial \tilde{n}} + \frac{\tilde{r} \cdot \tilde{n}}{\tilde{r}} \left(\frac{\tilde{\phi}}{\tilde{r}} + \frac{\dot{\tilde{\phi}}}{\tilde{a}} \right) \right]^{\tau^*} d\tilde{\mathbf{y}} =$$

$$\begin{cases} \tilde{\phi}(\tilde{\mathbf{x}}, \tilde{t}) &, \text{ for } \mathbf{x} \text{ in field} \\ \frac{1}{2}\tilde{\phi}(\tilde{\mathbf{x}}, \tilde{t}) &, \text{ for } \mathbf{x} \text{ on wing} \\ 0 &, \text{ for } \mathbf{x} \text{ ins ide wing} \end{cases}$$
 (2.2)

where $\tau^* = \tilde{t} - \tilde{r}/\tilde{a}$, $\tilde{a} = \beta/M$, $\beta = \sqrt{1 - M^2}$, $\tilde{r} = |\tilde{\mathbf{x}} - \tilde{\mathbf{y}}|$, and tildes denote evaluation in the Prandtl-Glauert space—

$$\left(\tilde{\mathbf{x}}, \tilde{t}\right) = \left(\frac{x_1}{\beta}, x_2, t - \frac{M^2 x_1}{\beta^2}\right). \tag{2.3}$$

Equation (2.2) is solved numerically by applying a zeroth-order boundary element method and linear time interpolation to give a set of algebraic equations¹⁴

$$H\phi_i^n = \sum_j G_{D_{ij}}^{(B)} \phi_j^{n-\tau_{ij}} - G_{S_{ij}}^{(B)} v_{n_j}^{n-\tau_{ij}}$$

$$+G_{R_{ij}}^{(B)}\dot{\phi}_{j}^{n-\tau_{ij}}+G_{D_{ij}}^{(W)}\Delta\phi_{j}^{n-\tau_{ij}},$$
 (2.4)

where,

$$\tau_{ij} = \frac{M}{\beta} \left(r_{\beta_{ij}} + M r_{1ij} \right), \qquad (2.5)$$

$$r_{\beta_{ij}} = \sqrt{(x_{i_1} - y_{j_1})^2 / \beta^2 + (x_{i_2} - y_{j_2})^2}.(2.6)$$

The indices i, j, and n refer to the collocation point, panel index, and time iteration, respectively. The blade and wake surfaces are denoted by (B) and (W), and G_S , G_D , and G_R refer to the source, doublet and ratelet influence matrices. By applying equations (2.4) to collocation points located at the center of each panel on the body, a time-domain solution for the surface distributions of ϕ is readily obtained. The flow velocity and pressure may then be determined through differentiation and Bernoulli's equation.

The solid surfaces of the blade section are impermeable. Thus, the normal perturbation velocity is required to satisfy

$$\mathbf{U}_{\infty} \cdot \mathbf{n} + \frac{\partial \phi}{\partial n} = 0. \tag{2.7}$$

The wakes are modeled as infinitely thin shear layers and, therefore, cannot support a pressure jump. By applying Bernoulli's equation to a point \mathbf{x}_+ just above and \mathbf{x}_- just below the wake, one obtains

$$\frac{\partial \Delta \phi}{\partial t} + \frac{1}{2}(v_{+}^{2} - v_{-}^{2}) = \frac{\partial \Delta \phi}{\partial t}
+ \frac{\mathbf{v}_{+} + \mathbf{v}_{-}}{2}(\mathbf{v}_{+} - \mathbf{v}_{-}) \qquad (2.8)$$

$$= \frac{D_{w}}{Dt}(\Delta \phi) = 0, \qquad (2.9)$$

where

$$\frac{D_w}{Dt} = \frac{\partial}{\partial t} + \mathbf{v}_w \cdot \nabla = \frac{\partial}{\partial t} + \frac{\mathbf{v}_+ + \mathbf{v}_-}{2} \cdot \nabla. \quad (2.10)$$

Equation (2.9) relates the wake strength $\Delta \phi$ to the potential jump at the trailing edge when the wake element was located at that trailing edge. Additionally, the wake evolution is determined such that the fluid elements in the wake are convected with the average velocity across the sheet. This defines a free-wake evolution which is described in greater detail in Wood and Grace¹⁵ and Ramsey.¹⁶ The free-wake evolution is easily implemented assuming incompressible flow (M=0).

Method Validation

To determine whether the current BEM calculation was working correctly for the BVI problem, a flat-plate airfoil simulation was run and compared to the analytical solution. The analytical lift response of a flat plate to a passing vortex is given by

$$\rho, \frac{c}{2}e^{-kh}(-iS(k))$$
 (2.11)

where $k=\frac{\omega c}{2U}$ is the normalized frequency, c is the chord length, U is the freestream speed far upstream, h is as defined in the previous section, , is the

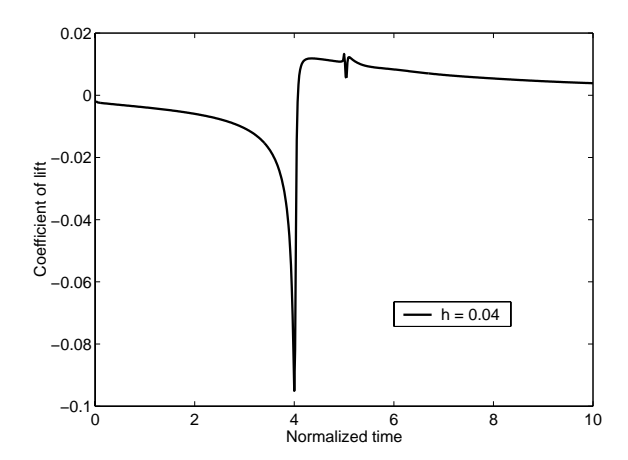


Fig. 4 Coefficient of lift vs. time for vortex passing flat plate at two different distances.

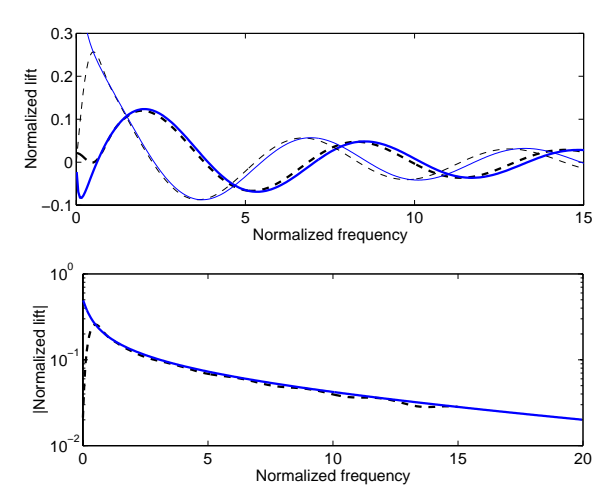


Fig. 5 Top: Real (thick line) and imaginary (thin line) part of Fourier transform for the analytical result (solid line) and the computed result (dashed line). Bottom: analytical magnitude of the response (solid) and the computed response (dashed).

strength of the vortex, and $i = \sqrt{-1}$, and S(k) is the Sears function, Eq. (1.1).

The flat plate was simulated using a NACA 0001 blade section. The vortex amplitude was 2% of the freestream and the vortex is introduced 4 chordlengths upstream. The vortex passes above the flat plate at a distance of 4% of the half chord. Figure 4 shows the computed lift response. The real and imaginary part of the lift spectrum as well as its magnitude is compared against the analytical solution in Figure 5. The agreement between the computed and analytic results is very good, but error exists at low frequency where the singular behavior is not captured using the BEM method (due most likely to the finite time of computation).

Experimental BVI data reported in the literature^{2,17} is used to obtain a second qualitative validation of the computation. In the experiment, a NACA 0012 blade was instrumented with several

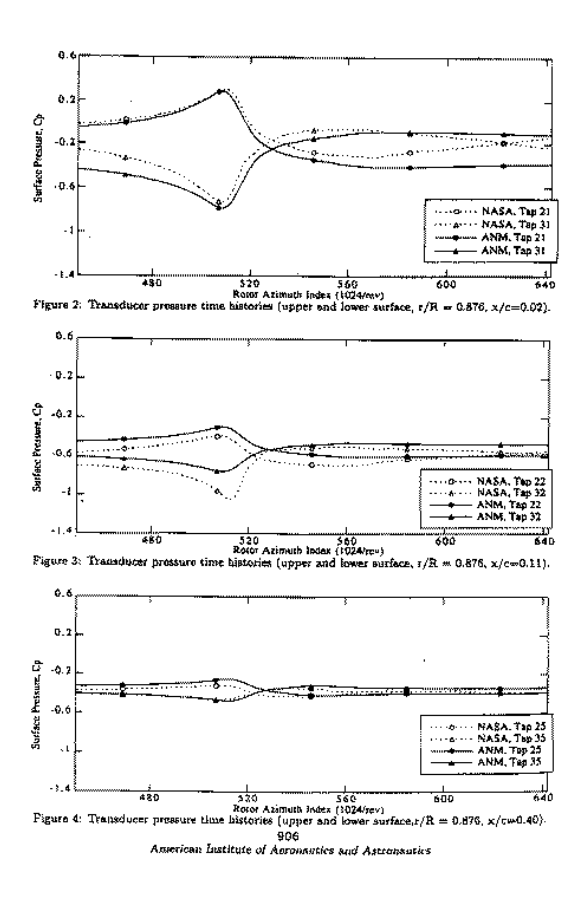


Fig. 6 Reproduced from [Ref.17]. Coefficient of pressure in time as vortex passes the blade section.

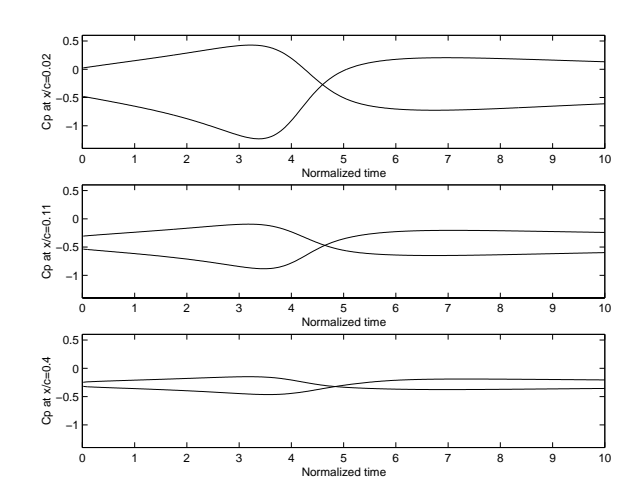


Fig. 7 Coefficient of pressure from NACA 0012 simulation with vortex of strength 1.0 passing at a distance of 1 chord.

pressure taps and rotated as a helicopter rotor at no mean angle of attack. As the blade encountered a vortex generated from the tip of another stationary blade, the surface pressure was recorded. In [Ref.4] the data were presented on a normalized and shifted scale. In [Ref.17], the data were plotted on a different scale which probably reflects the actual values. The plot has been reproduced in Figure 6; the experimental data is denoted by the dotted line. In neither report was the meaning of the independent axis clearly explained. Finally, the actual value of the vortex strength is not easily determined. Thus, this data is only used for qualitative comparisons in this paper.

The most noticeable feature in the experimental data, is the asymmetry in the unsteady pressure from top to bottom of the blade. This asymmetry is reproduced by a generic simulation using the current computational method. Because the experimental parameters are not known, a vortex passing at 1 chord above the airfoil with strength 1.0 was simulated. The calculated surface pressure at the 3 chord locations of interest are shown in Figure 7. The asymmetry is apparent, but the pressure gradients along the chord are not as strong as they appear to be in the data. The predicted presure gradient will increase when the strength of the vortex is increased or the closest approach distance is decreased.

Effect of discretization

Reported BVI time domain lift signals, computed using boundary element methods, show a small blip at the time corresponding to the passage of the vortex past the trailing edge. ^{18,19} This blip is usually attributed to numerical accuracy and not investigated thoroughly. When one is interested in the lift spectrum however, such an investigation is necessary, as large gradients in the time signal can affect the details of the spectrum. In the current research the blip has been linked to panel size mismatch between the body panels near the trailing edge and the wake panels. This link is demonstrated in this section by example.

A NACA 0012 blade section whose chord is placed on the x-axis from from -0.5 to 0.5 is subject to a freely evolving vortex of nondimensional strength 0.02 imposed at an upstream location of (-4.5, 0.03). The freestream flow is normalized to unity. The vortex has a closest approach to the airfoil (based on half chord) of 0.038.

The lift response of the NACA 0012 was calculated using three different airfoil discretization methods and the results are shown in Figure 8. Linear spacing refers to equal spacing along the chord of the airfoil. Cosine spacing refers to an equal θ -space discretization where $-\frac{c}{2}cos\theta = x$. The mixed discretization

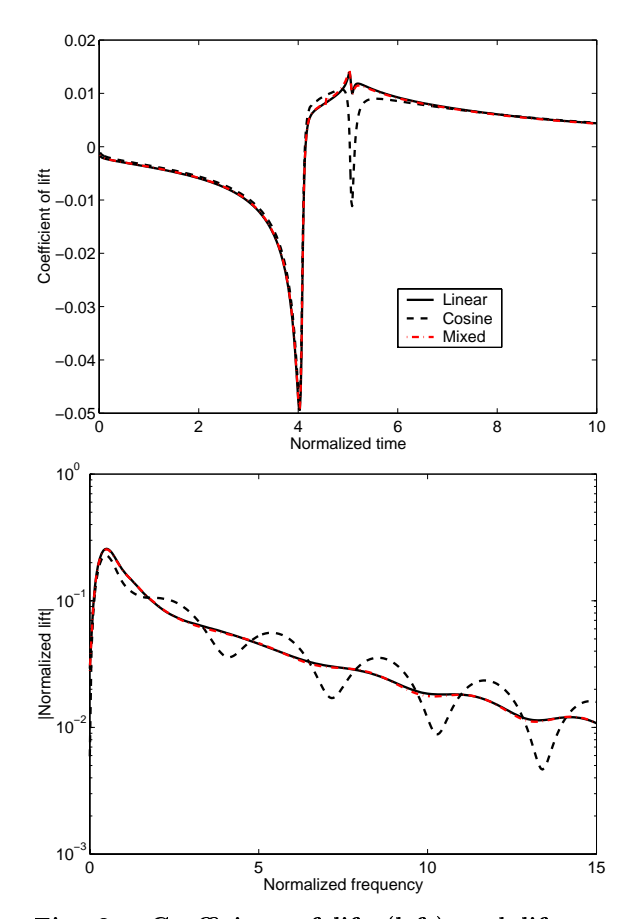


Fig. 8 Coefficient of lift (left) and lift spectrum (right) computed using different airfoil discretizations.

uses a cosine spacing from the midchord forward and a linear spacing from the midchord aft. It is clear from the response spectrum, that the cosine discretization which predicts a larger forced response as the vortex passes the trailing edge of the blade section also predicts a much more scalloped frequency spectrum. (t=5 corresponds to the vortex passing the trailing edge).

The main difference between the linear and cosine spacings is their compatibility with the wake spacing. In the current simulation, a wake panel is shed at every time step. These panels have a length, determined by the convection speed, i.e. approximately Udt. For the linear spacing, the body panels forward of the trailing edge are similar in length to the wake panels aft of the trailing edge. Body panels near the trailing edge determined from a cosine spacing however have lengths much shorter than the wake panels. It is this incompatibility in the panel spacings near the trailing edge which is responsible for the large blip in the lift response; and it is this blip in the time signal that leads to the large oscillations in the lift spectrum.

Thus, the linear discretization seems best for computing BVI response within the current scheme.

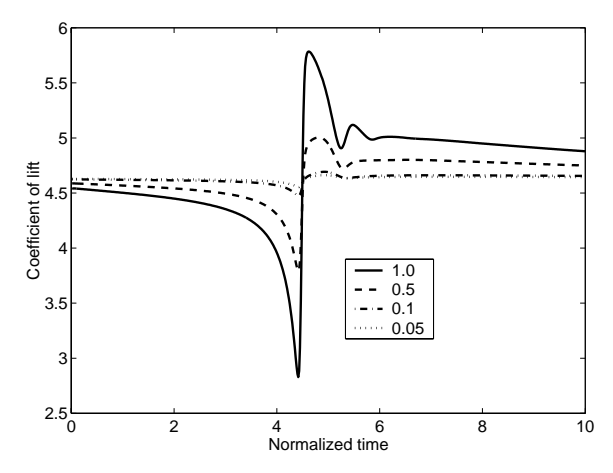


Fig. 9 Coefficient of lift for various vortex strengths. All vortices follow same streamline path.

However, linear discretization does not capture a leading edge pressure rise well. Therefore, the mixed panel spacing with cosine spacing near the leading edge and linear near the trailing edge has been adopted. Figure 8 shows that this discretization gives the same result as the linear discretization for the NACA 0012 case. It is noted that the mixed discretization gives better results for thinner cambered blade sections when compared to the linear discretization, because of the larger pressure rise at the leading edge.

Nonlinear Interactions

The gust model is based on rapid distortion theory (RDT) which requires that unsteady disturbances be treated as perturbations to the mean flow; and as such, the time varying quantities can only be affected by mean flow quantities and solid surfaces. A time domain based BVI computation however does not have to rely on the RDT assumptions. stead, nonlinear interactions between the imposed vortex, the generated wake vorticity, and what can be thought of as image vortices inside the blade can be easily modeled. Using the current methodology, it is easy to assess the implication of imposing the RDT assumption on a BVI calculation. In particular, the vortex can be forced to follow a streamline as it passes the airfoil as opposed to being allowed to evolve freely. Results from such a computation are discussed here.

A Joukowski blade section of chordlength 2.0 formed using parameters $S_R = -0.1$ and $S_I = 0.2$ at 20° angle of attack was subjected to passing vortices of differing strengths. Each vortex was forced to follow the streamline that had a closest approach distance of 8% of the half chord. The lift response is shown in Figure 9. If the RDT assumption were valid, the lift curves would collapse when scaled by the vortex strength:

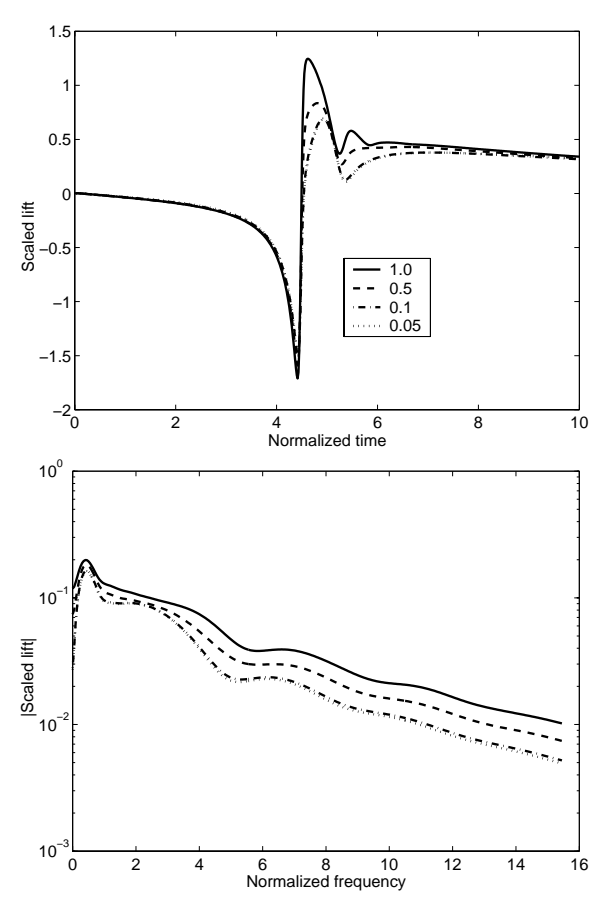


Fig. 10 Normalized lift vs. time (left) and vs. frequency (right) for various vortex strengths. All vortices follow same streamline path.

scaled lift =
$$\frac{C_l - C_{l_0}}{\cdot}$$
 (3.1)

where the subscript 0 denotes the steady (i.e. initial) coefficient of lift. The scaled lift in time and its spectrum are shown in Figure 10. For cases where the vortex strength is less than 10% of the freestream (i.e. vortex strength ≤ 0.1), the results collapse.

A scaling rule is often used to determine whether a method based on RDT is applicable for analysis of a given physical phenomenon. To be applicable, the disturbance amplitude should be less than 10\% of the mean flow. In the current example, it is only a coincidence that the RDT validity cut off comes about for vortex strengths that are roughly 10% of the freestream because it is the influence of the vortex in the region near the blade that determines the important disturbance scale. Therefore, for the BVI problem, the passing distance is as important as the vortex strength. In this example, the vortex passes at a distance equivalent to roughly 10% of the halfchord. This result can be generalized to say that vortices with strength n% of the freestream passing less than n% of a halfchord away from the blade

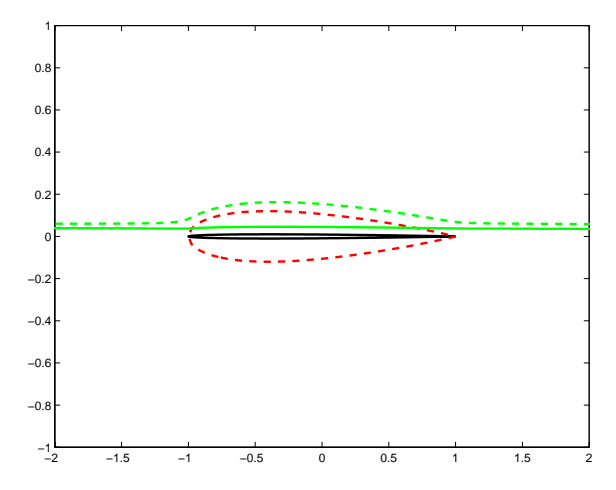


Fig. 11 Response of the airfoils in time and their associated response spectrum.

must be simulated using free vortex evolution as opposed to an RDT approach.

Effect of blade thickness

Comparison of the response to a passing vortex of two blade sections: a NACA 0001 and a NACA 0012 shows that as thickness increases, the response especially at high frequencies decreases. These BVI simulations were performed with a vortex initial location such that the vortex passed with a closest distance of 4% of a half chord. The geometries and their associated vortex paths are shown in Figure 11. The coefficient of lift for the two simulations is shown as well as the lift spectrum in Figure 12. The response of the NACA 0012 is several dB less than that of the NACA 0001 at higher frequency.

A set of Joukowski blade sections with varying thickness were also tested. The blade sections appear in Figure 13. The flow was set to an incidence angle of 20° and the closest passing distances for the different blade sections were $0.025,\,0.04,\,0.044,\,0.037$ respectively. The corresponding responses are given in Figure 14. The steady lift has been factored out so comparison of the unsteady response can be made. It is clear that the response of the blade section decreases with increased thickness.

The reduction in response with thickness is attributed to two causes. First, the magnitude of the induced normal wash due to the passing vortex is identical from pressure to suction side for the flat plate; but, for the thicker airfoil, the side closest to the passing vortex is influenced more strongly by the vortex. Second, the phase of the incident downwash along the flat plate is identically $e^{-ik_1x_1}$; but, for the thicker airfoil, there is a departure from this predictable phase variation. Both of these effects are evident in Figures 15 and 16 where the magnitude and $e^{ik_1x_1} \times \text{phase}$ of the incident velocity along the chord of the NACA 0001 and 0012 airfoils are plotted

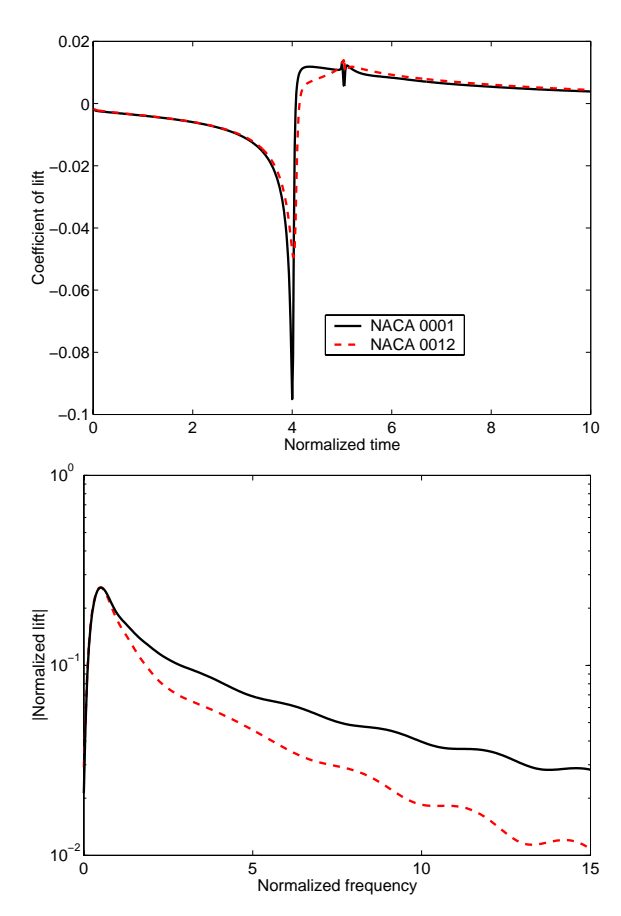


Fig. 12 Response of the airfoils in time and their associated response spectrum.

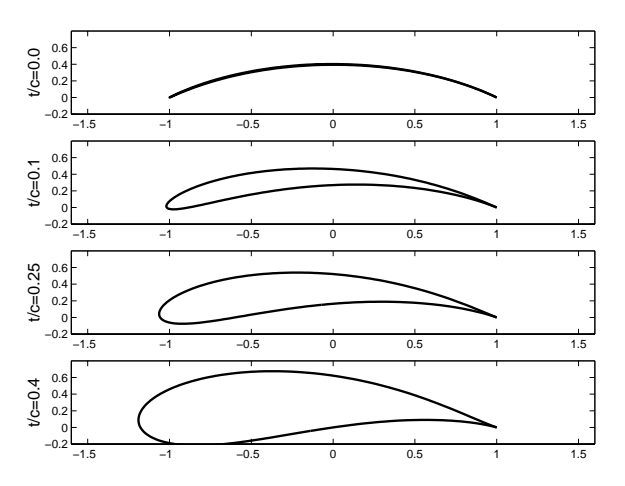


Fig. 13 Airfoils used in thickness simulation.

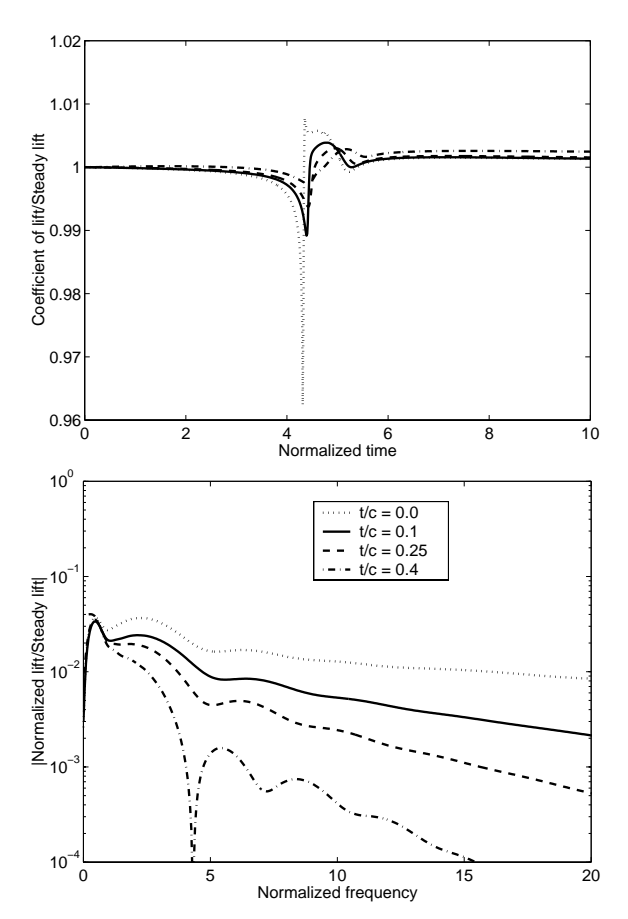


Fig. 14 Response of the airfoils in time and their associated response spectrum.

at several frequencies. (The normalized frequency is noted to the left of each curve.)

The surface pressure resulting from the induced wash is also asymmetric from pressure to suction side for the thicker airfoil as seen in Figure 17. In addition, at higher frequency, the phase of the pressure is quite different along the chord of the NACA 0012 airfoil, Fig. 18. The total lift is obtained by integrating the pressure jump along the body. Thus when the induced flow on the suction and pressure sides are simply π out of phase at each chordwise location and identically phased with $e^{-ik_1x_1}$, the maximum lift will be obtained. In the other cases shown, the lift will be less.

The phase of the incident velocity along the chord of a thick airfoil due to a transverse gust will vary from the flat plate canonical form $(e^{-ik_1x_1})$ in the frequency domain similarly to that shown for the BVI case. However, for a symmetric, thick, blade section shape, the magnitude of the induced wash will be the same on both the pressure and suction sides. The method for introducing asymmetry from side to side is the introduction of a longitudinal gust

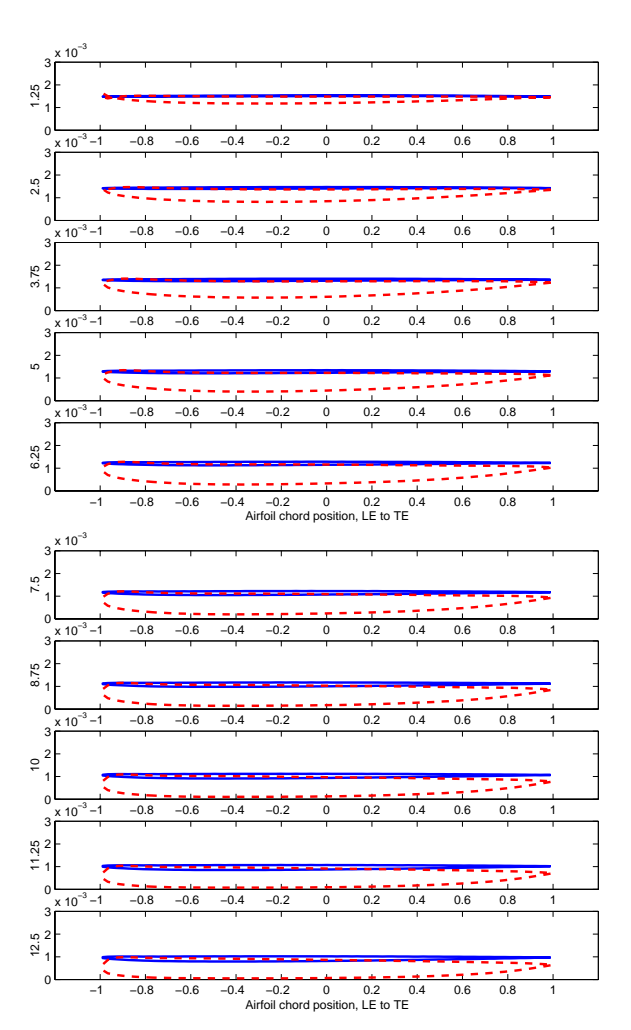


Fig. 15 Magnitude of induced velocity along the blade section at various normalized frequencies. NACA 0001: solid line, NACA 0012: dashed line.

component. This gust component is often left out of the frequency domain gust simulations. Moreover, to fully capture the correct asymmetry, multiple longitudinal wave numbers must be computed for each transverse wave number.

Conclusions

It is shown that the decrease in response with increased blade thickness that has been reported experimentally is a result of both an increased asymmetry in the lift distribution from top to bottom of the blade as well as an increased phase variation in the surface pressure along the chord. Such surface pressure distributions are inherently captured in time domain BVI calculations; whereas, a gust approach would require multiple longitudinal wave number response calculations in order to model the asymmetry. In addition, it was shown that a time domain BVI calculation can easily incorporate nonlinear motion of the passing vortex which cannot be incorporated in a frequency domain BVI simulation or in a gust based computation. However, the

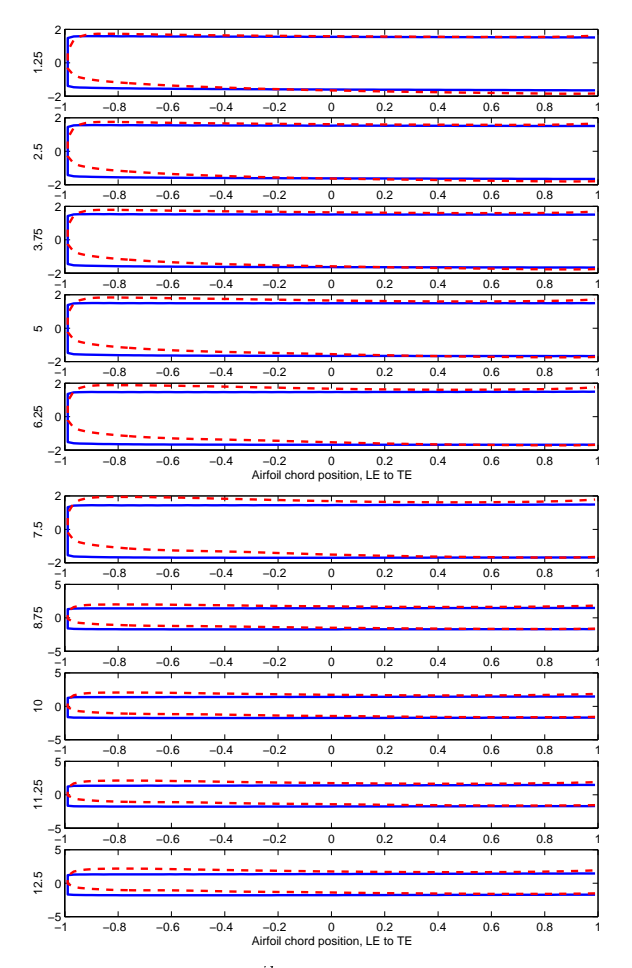


Fig. 16 Phase * $e^{ik_1x_1}$ of induced velocity along the blade section at various normalized frequencies. NACA 0001: solid line, NACA 0012: dashed line.

gust based model does have one strong advantage that was not highlighted in this paper. General flow disturbances that may be known from experimental measurement can be described as a series of gusts by simply analyzing the field's Fourier transform. It is much harder to produce a group of discrete vortices whose influence on a solid body in the flow is similar to the real flow disturbances influence.

Acknowledgements

The author would like to acknowledge the ASEE Summer Faculty Research program, under which much of this work was completed. In addition, gratitude is extended to Robert Minniti of David Taylor Model Basin, and Doug Dahmer of NAVSEA 93R who supported the research. Finally, the initial impetus to conduct this research came from interactions with Rudolph Martinez of Cambridge Acoustical Associates and much of the code development is attributed to Luigi Morino, visiting professor at BU, and Trevor Wood, a graduate research assistant at Boston University.

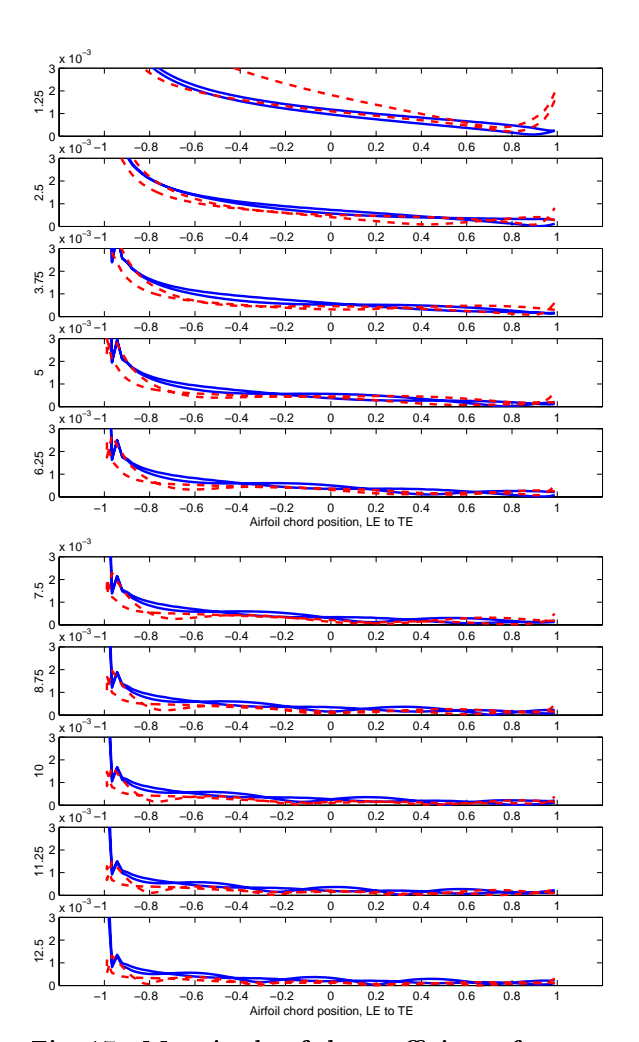


Fig. 17 Magnitude of the coefficient of pressure along the blade section at various normalized frequencies. NACA 0001: solid line, NACA 0012: dashed line.

References

¹Hassan, A. A., Straub, F. K., and Charles, B. D., "Effects of Surface Blowing/Suction On The Aerodynamics of Helicopter Rotor Blade-vortex Interactions (BVI) - A Numerical Simulation," *J. of the American Helicopter Society*, Vol. 42, No. 2, April 1997, pp. 182–194.

²Kitaplioglu, C., Caradonna, F., and Burley, C. L., "Parallel Blade-vortex Interactions: An Experimental Study and Comparison with Computations," *J. of the American Helicopter Society*, Vol. 42, No. 3, July 1997, pp. 272–281.

³Martinez, R., Rudzinsky, J., and Atassi, H. M., "Analytic Evaluation of Shape Effects on Blade-Vortex Interaction," Tech. Rep. U-2466-402.14, Cambridge Acoustical Associates, Dec. 1997.

⁴Caradonna, F., Kitaplioglu, C., McCluer, M., Baeder, J., Visintainer, J., Bridgeman, J., Epstein, R., Lyrintzis, A., Koutsavdis, E., Rahier, G., Delrieux, Y., Rule, J., and Bliss, D., "Methods for the Prediction of Blade-Vortex Interaction Noise," J. of the American Helicopter Society, Vol. 45, No. 4, October 2000, pp. 303–317.

⁵Atassi, H. M., "Unsteady Aerodynamics and Vortical Flows: Early and Recent Developments," *Aerodynamics and Aeroacoustics*, edited by K. Y. Fung, World Scientific, Singapore, etc., 1994, pp. 119–169.

⁶Agarwal, R. K. and Huh, K. S., "Acoustic Radiation due to Gust-Airfoil Interaction in a Compressible Flow," *AIAA Paper No. 96-1755*, 1996.

⁷Grace, S. M., Hariharan, S. I., and Atassi, H. M., "Direct Computations of Unsteady Flows About Thin Airfoils,"

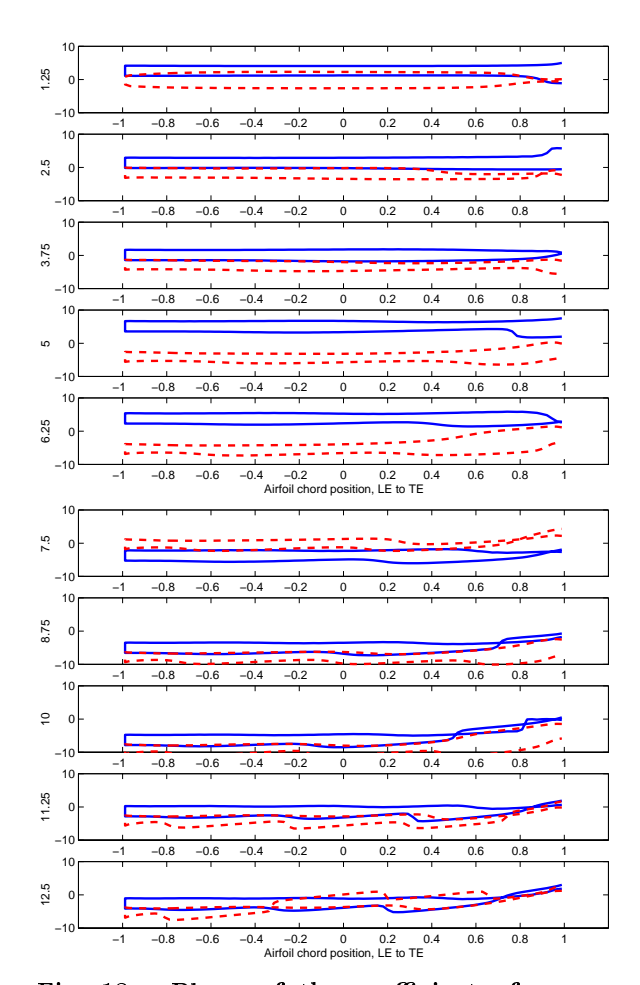


Fig. 18 Phase of the coefficient of pressure along the blade section at various normalized frequencies. NACA 0001: solid line, NACA 0012: dashed line.

 $Journal\ of\ Computational\ Acoustics,\ Vol.\ 6,\ No.\ 3,\ 1998,\ pp.\ 337-355.$

⁸Lockard, D. P. and Morris, P. J., "Radiated Noise from Airfoils in Realistic Mean Flows," AIAA Journal, Vol. 36, No. 6, june 1998, pp. 907–914.

⁹Olsen, W. and Wagner, J., "Effect of Thickness on Airfoil Surface Noise," *AIAA J.*, Vol. 20, No. 3, March 1982, pp. 437–439.

 $^{10}\mathrm{Minniti,\ R.,\ 2000,\ private\ communication\ with\ DTMB\ research\ scientist.}$

¹¹Morino, L., "A General Theory of Unsteady Compressible Potential Aerodynamics," Tech. Rep. CR-2464, NASA, 1973

¹²Gennaretti, M., Luceri, L., and Morino, L., "A Unified Boundary Integral Methodology for Aerodynamics and Aeroacoustics of Rotors," J. Sound and Vib., Vol. 200, No. 4, 1997, pp. 467–89.

 $^{13}{\rm Morino,~L.,~"Boundary~Integral~Equations~In~Aerodynamics,"}$ Appl.~Mech.~Rev., Vol. 46, No. 8, 1993, pp. 445–66.

¹⁴Morino, L. and Tseng, K., "Steady, Oscillatory and Unsteady, Subsonic and Supersonic Aerodynamics (SOUSSA) For Complex Airfcraft Configurations," *Unsteady Aerodynamics*, 1977, AGARD CP-273.

¹⁵Wood, T. H. and Grace, S. M., "Free-Wake Analysis for Calculating the Aeroacoustics of a Wing-Flap Configuration," Proceedings of the 38th AIAA Aerospace Sciences Meeting, Reno, NV, Jan 10-13 2000, pp. 162–173, Paper no. AIAA 2000-0607.

¹⁶Ramsey, W. D., Boundary integral methods for Lifting Bodies with Vortex Wakes, Ph.D. thesis, Massachusetts Institute of Technology, Cambridge, Massachusetts, 1996. ¹⁷Rule, J. A., Epstein, R. J., and bliss, D. B., "An Analytical/Numerical Matching - Turbulent Core Model Blade Vortex Interaction Study," *Paper 97-1707-CP*, 1997.

 $^{18}{\rm Lee,\,Y.\,T.,\,Feng,\,J.,\,and\,Merkle,\,C.\,L.,\,"Time-dependent Inviscid Flow Analysis of Rotor-stator Systems,"$

¹⁹Chow, C. Y. and Huang, M. K., "Unsteady Flows about a Joukowski Airfoil in the Presence of Moving Vortices," 1983.